Miniature paleo-speleothems from the earliest Ediacaran (635 Ma) Doushantuo cap dolostone in South China and their implications for terrestrial ecosystems

Tian Gan[1,2,3,4], Guanghong Zhou[5,6*], Taiyi Luo[1*], Ke Pang[3,4], Mingzhong Zhou[7], Weijun Luo[8], Shijie Wang[8], Shuhai Xiao[2*]

[1] State Key Laboratory of Ore Deposit Geochemistry, Institute of Geochemistry, Chinese Academy of Sciences, Guiyang 550081, China

[2] Department of Geosciences, Virginia Tech, Blacksburg, VA 24061, USA

[3] State Key Laboratory of Palaeobiology and Stratigraphy, Nanjing Institute of Geology and Palaeontology and Center for Excellence in Life and Paleoenvironment, Chinese Academy of Sciences, Nanjing, 210008

[4] University of Chinese Academy of Sciences, Beijing 101408, China

[5] School of Geography and Resources, Guizhou Education University, Guiyang 550018, China

[6] Guizhou Provincial Key Laboratory of Geographic State Monitoring of Watershed, Guizhou Education University, Guiyang 550018, China

[7] School of Geographical and Environmental Sciences, Guizhou Normal University, Guiyang 550001, China

[8] State Key Laboratory of Environmental Geochemistry, Institute of Geochemistry, Chinese Academy of Sciences, Guiyang 550081, China

*E-mail address: zhouguanghong@gznc.edu.cn; luotaiyi@vip.gyig.ac.cn; xiao@vt.edu.

ABSTRACT

Speleothems can offer insights into terrestrial life because their formation is critically dependent on soil-microbial ecosystems. Here we report the wide distribution of miniature paleo-speleothems from the ~635 Ma Doushantuo cap dolostone in South China in order to understand the recovery of terrestrial life after the terminal Cryogenian Marinoan snowball Earth glaciation. The cap dolostone was deposited during the initial transgression following deglaciation, but subsequently developed extensive karstic cavities or sheet-cracks when the cap dolostone was brought to the phreatic zone during post-glacial rebound. The sheet-cracks were filled with multiple generations of cements, including isopachous dolomite formed in the phreatic zone and speleothems formed in the vadose zone. The paleo-speleothems are millimeters-centimeters in size and include stalactites, stalagmites, helictites, moonmilk, flat crusts, and botryoids. The speleothems were silicified by subsequent hydrothermal processes, which also precipitated the chalcedony and quartz in the sheet-cracks and occurred before a renewed transgression in which ~632 Ma shales overlying the cap dolostone were deposited. The wide distribution of paleo-speleothems indicates the presence of an active soil-microbial ecosystem in the earliest Ediacaran Period and in the aftermath of the Marinoan snowball Earth.

INTRODUCTION

The Cryogenian Marinoan snowball Earth glaciation (ca. 650–635 Ma) likely had a catastrophic impact on both the marine and terrestrial ecosystems (Hoffman et al., 2017). Post-glacial recovery of the marine ecosystem is evidenced by the presence of microbialites (Romero et al., 2020) and eukaryotic biomarkers (van Maldegem et al., 2019) in cap dolostone immediately overlying Cryogenian glacial deposits. The recovery of non-marine ecosystems in lacustrine, fluvial, and terrestrial environments, on the other hand, has not been investigated, although geochemical (Kennedy et al., 2006; Knauth and Kennedy, 2009; Kump, 2014) and paleontological data (Horodyski and Knauth, 1994; Strother et al., 2011; Wellman and Strother, 2015) suggest that these environments had been colonized prior to the Cryogenian Period. The recovery of terrestrial ecosystems is particularly important for the well-being of the entire biosphere, because they facilitate the liberation of bio-available nutrients from minerals (van der Heijden et al., 2008) and the supply of these nutrients to the marine realm (Thomazo et al., 2018).

Karstic deposits, particularly speleothems, are terrestrial deposits that can archive remarkable paleoenvironment records (Verheyden et al., 2000; McDermott, 2004; Fairchild et al., 2006). Studies of modern karstic caves suggest that speleothem deposition is mostly controlled by the evolution of CO_2 contents in drip-waters, which originate from meteoric precipitation at equilibrium with atmospheric CO_2 and then become CO_2-supersaturated when interacting with soil-microbial systems where microbial respiration and organic decomposition led to CO_2 enrichment, followed by CO_2 degassing in caves (Dörr and Münnich, 1986; Baker et al., 1996; Frisia and Borsato, 2010). Thus, paleo-speleothems, such as dripstones (Amodio et al., 2018), micro-stalactites (Freytet and Verrecchia, 2002; Qing and Nimegeers, 2008), and stromatolitic coatings (Álvaro and Clausen, 2010), are important evidence for subaerial exposure and paleo-pedogenesis.

The extensive karstic surface atop the 635 Ma cap dolostone in Africa, Canada, and South China (James et al., 2001; Shields et al., 2007; Zhou et al., 2010), offers a rare opportunity to explore paleo-speleothems in order to illuminate the terrestrial ecosystems in the aftermath of the Marinoan snowball Earth glaciation. In this paper, we report miniature paleo-speleothems (including stalagmites, stalactites, helictites, moonmilk, flat crusts, and botryoids) preserved in the karstic sheet-cracks in the 635 Ma cap dolostone of the basal Ediacaran Doushantuo Formation in South China. These paleo-speleothems not only confirm the post-glacial isostatic rebound event as documented previously, but also indicate a rapid re-establishment of the terrestrial soil-ecosystem following deglaciation.

GEOLOGICAL SETTING

The early Ediacaran Doushantuo Formation was deposited on a passive continental margin on the Yangtze Block of South China (Fig. DR 1). It overlies the terminal Cryogenian Nantuo Formation, which consists of glacial diamictite ranging from a few meters thick in shallow-water platform facies to >1000 m thick in basinal facies (Zhou et al., 2010). The Doushantuo Formation begins with a 3–5 m thick cap dolostone, which was deposited at ca. 635 Ma in a $<10^6$ yr interval during the initial transgress following deglaciation (Zhou et al., 2010; Zhou et al., 2019). The cap dolostone contains abundant sheet-cracks (Jiang et al., 2006) and is capped by an extensive karstification surface in South China (Zhou et al., 2010). The sheet-cracks are interpreted as karstic cavities that were formed through interaction with meteoric water in the phreatic zone when the cap dolostone was subaerially exposed due to post-glacial rebound (Zhou et al., 2010).

METHODS

Sheet-crack samples were collected from five sections across the Yangtze Platform (Fig. DR 1). Fifteen of these samples were subjected to petrographic analysis, including one (ZCP-1) from the Zhangcunping section (N31°17′34″, E111°12′30″) and three (14XFH-1, 14XFH-3, and 14XFH-5) from the Xiaofenghe section (N30°48′54″, E111°03′20″) in Hubei Province, three (14DPc1-1, 14DPc1-2 and 14DPc1-3) from the Daping section (N28°59′01″, E110°27′42″) in Hunan Province, and four (16WH-1, 16WH-2, 16WH-3, and 16WH-4) from the Wenghui section (N27°49′55″, E109°01′32″) and four (18BDS-2, 18BDS-4, 18BDS-7, and 18BDS-9) from the Beidoushan section (N27°01′40″, E107°23′22″) in Guizhou Province. Petrographic thin sections (100 μm and 200 μm thick) and polished slabs were cut perpendicular or parallel to the bedding plane and were investigated using transmitted light microscopy (TLM), reflected light microscopy (RLM), epifluorescent light microscopy (ELM), and backscattered scanning electron microscopy (BSEM).

PALEO-SPELEOTHEMS

Sheet-cracks in the cap dolostone are filled with a consistent sequence of cements, which start with isopachous dolomite (ID; sometimes with barite), followed by siliceous minerals (chalcedony and quartz), and end with blocky calcite and barite (Zhou et al., 2017b). The ID fabric is regarded as early-stage cement precipitated in the phreatic zone where meteoric water and sea water mixed, because ID is distinguished by coarse euhedral dolospar (ca. 500 μm long) with straight crystal edge and Middle-REE enrichment model with Fe/Mn decrease from early to late stage (Unpublished data). The blocky calcite phase, characterized with extremely negative $\delta^{13}C_{carb}$ values, are regarded as late-stage cement (Zhou et al., 2010). Paleo-speleothems described here occur in the intermediate phase and most of them are silicified with a chalcedony although some are partially silicified with residual calcareous fabrics (Fig. DR 2). Based on comparison with modern speleothems (Banks and Jones, 2012) and following terminology in modern speleology, the Doushantuo paleo-speleothems are regarded as microspeleothems and described under six morphological types, including stalactites, stalagmites, helictites, moonmilks, flat crusts, and botryoids (Figs. 1–4; Fig. DR 2B).

Stalactites occur in sheet-cracks at Beidoushan and Wenghui (Figs. 1, 2A, 2D, 2F). They hang downwards from the ceiling of sheet-cracks and occur either singularly or as coalesced multi-stalactites. Individual stalactites are 3–8 mm in diameter and 1–30 mm in length. A stalactite typically consists of a "soda-straw" drip channel in the center (Figs. 1B–D, 2D), which is ~100 μm in diameter, lined with brown organic material, and filled with cryptocrystalline chalcedony. The drip channel is surrounded by a layer of fibrous chalcedony about 400–500 μm thick and then alternating organic-rich and organic-poor chalcedony laminae each about 20 μm thick (Figs. 1B–D). Some of these laminae appear botryoidal in shape (best seen in longitudinal sections, e.g., Fig. 1C), reflecting stable and slow feeding of ground water. The outermost laminae are typically thicker (100–200 μm thick; Fig. 1C).

Stalagmites, which grow upwards from the floor of sheet-cracks, were found at Wenghui, Xiaofenghe, and Beidoushan (Figs. 2A–B, 2D–E, 3E). Different from stalactites, stalagmites do not have a "soda-straw" drip channel. They taper distally, with a diameter of ca. 5–13 mm in diameter and a length of ca. 10–35 mm, thus representing "minimum-diameter" stalagmites (Fairchild and Baker, 2012) formed in microkarst such as sheet-cracks where drip fall heights are short (Gams and Beck Barry, 1981). A longitudinal section shows that the stalagmite starts with a stacked mamillary structure (Fig. 2B), which is typically observed at the bottom of modern stalagmites (Baker et al., 1993; Tan et al., 2006; Tan et al., 2013; Railsback et al., 2018) and represents turbulence of dripping water at the beginning of stalagmite deposition (Dreybrodt and Romanov, 2008). Later growth is characterized by more continuous, smooth, and alternating organic-rich and organic-poor laminae each 20–40 μm in thickness (total ~2 mm in thickness, Fig. 2C), similar to modern calcareous stalagmites (Baker et al., 1993; Tan et al., 2013; Railsback et al., 2018). In one example, a stalagmite meets a stalactite (Fig. 1A), forming a stalagnate (Gribovszki et al., 2017) that extends from the ceiling to the floor of a sheet-crack. Although most stalagmites are silicified with a chalcedony fabric, those from Xiaofenghe are partially silicified, with residual calcite core and laminae (Fig. 3E).

Elongate helictites growing obliquely in random directions were observed at Beidoushan (Figs. 3A–B). They can be vermiform, filiform, ramiform, straight, curved, or twisted. They are typically ca. 1–2 mm long and 200–300 μm wide. A narrow central canal 10–20 μm in diameter occurs in the center of helictites (Fig. 3B, arrows). The helictites typically consist of an inner zone (100–200 μm wide) of homogenous cement and an outer zone (50–100 μm wide) of laminae enriched in clay and organic matter.

Moonmilk at Beidoushan appears as a laterally continuous botryoidal crust on sheet-crack walls (Figs. 3C–D). Moonmilk typically consists of a microcrystalline core (a few μm thick) and an outer shell (~500 μm thick) with alternating organic-poor and organic-rich laminae, similar to Holocene moonmilk from the Grotta Cesare Battisti cave, North Italy (Borsato et al., 2007). Filamentous microfossils are preserved in the microcrystalline core (Figs. 3C–D, arrows), reminiscent of filamentous micro-organisms in modern moonmilk (Cañaveras et al., 2006; Baskar et al., 2011).

Flat crusts are common in sheet-cracks observed in this study (Figs. 1A, 2A–C, 3A, 4A–C). Previously described as isopachous aggregates (Zhao et al., 2018), flat crusts are typically continuously flat or slightly wavy isopachous cements, ca. 0.1–10 mm thick, on sheet-crack walls (Figs. 4A–C) and sometimes intergrading laterally to stalactite (Figs. 1A, 2A), stalagmites (Figs. 2A –B) and helictites (Fig. 3A). They consist of alternating organic-poor and organic-rich laminae each about 20–60 μm thick (Figs. 2C, 4C).

Botryoids up to 5 mm in size are found coating on sheet-crack walls at Zhangchunping, Beidoushan, and Daping (Figs. 4D–H). Typically, botryoids start with aggregates of clotted material that are covered with alternating organic-rich and organic-poor laminae (Figs. 4E–F). Partially silicified botryoids show that the laminae were originally calcareous (Figs. 4F–G).

DISCUSSION

Modern siliceous speleothems can be either primary (Aubrecht et al., 2008) or secondary (Skotnicki and Knauth, 2007). Primary or protogenetic siliceous speleothems developed in caves or lava tunnels overlain by silicate rocks such as quartzites, sandstones, or igneous rocks (Aubrecht et al., 2008). Although the Member II black shale overlying the cap dolostone in the Doushantuo Formation (Cao et al., 1989) could in principle be a silica source for the siliceous paleo-speleothems described in this paper, this scenario is inconsistent with the lack of karstic features in the black shale. Instead, we suggest that the Doushantuo paleo-speleothems are secondary. In other words, they were originally calcareous speleothems but later silicified by low-temperature hydrothermal processes. This interpretation is consistent with partially silicified paleo-speleothems from Daping (Figs. 4F, 4G) and Xiaofenghe (Fig. 3E), where residual calcareous laminae are preserved.

Although the Doushantuo paleo-speleothems are secondarily silicified, there is evidence suggesting that both speleothem precipitation and secondary silicification occurred sometime between 635 Ma and 632 Ma. Zhou et al. (2010) recognized three events associated with the Doushantuo cap dolostone : (1) postglacial transgression and cap dolostone deposition at ca. 635 Ma (Zhou et al., 2019); (2) isostatic rebound and cap dolostone karstification; and (3) renewed transgression and deposition of Doushantuo Member II black shale, which dates to 632 Ma (Condon et al., 2005). Because the Doushantuo Member II is not karstified, the second event (cap dolostone karstification and speleothem formation) is constrained between 635 Ma and 632 Ma.

Further evidence suggests that karstification, speleothem formation, and secondary silicification all occurred around 635 Ma. First, the top of the cap dolostone represents a karstification surface and is covered by a volcanic ash dated at 635.2 Ma (Condon et al., 2005), placing a maximum age constraint on karstification. Second, the vertical length of the paleo-speleothems (10–35 mm) suggested an estimated duration of karstification around 3.5 ka. This estimated is based on a mean growth rate of 5.1 μm/yr for stalagmites in the last glaciation in southern Brazil (Cruz et al., 2006), a growth rate of ~10 μm/yer for stalagmites since the last glaciation in South China (Lin et al., 2005), speleothem growth rates of 9–14 μm/yr and 7.4–11.2 μm/yr during the late Pleistocene deglaciation period in Brazilian subtropics (Cruz et al., 2006). Third, although the chalcedony fabric of the silicified paleo-speleothems and the silica phase filling the space in between are both regarded as low-temperature hydrothermal precipitates based on fluid-inclusion homogenization temperatures (Zhou et al., 2017b), trace element features such as low Ge/Si ratios, depleted LREE patterns, and positive Eu anomalies in the silica phase indicate a mixture of marine and hydrothermal silicon source (Cui et al., 2019), suggesting that speleothem silicification probably occurred during the early stage of the second transgression shortly after 635.2 Ma.

Doushantuo paleo-speleothems described here have modern analogs, which include gravitational and non-gravitational speleothems (Banks and Jones, 2012). Gravitational speleothems such as stalactites and stalagmites are related to dripping water sourced from the epikarst. When the dripping water saturated with calcium carbonate flows out of fissures, it degasses and deposits a thin calcite film that contributes to the growth of stalactites and stalagmites (Baker et al., 1993; Tan et al., 2013; Railsback et al., 2018), with the alternating laminae representing the alternation between affluent and poor feeding or between stable and unstable precipitations (Brook et al., 1999; Baker et al., 2002; Tan et al., 2006). Doushantuo non-gravitational speleothems include helictites, moonmilk, botryoids, and flat crusts. Helictites may be related to hydrostatic pressure feeding capillary flow (Huff, 1940; Onuk et al., 2014), which is too slow to form a hanging droplet. The formation of modern moonmilk is probably driven by microbial-mediated nucleation and mineralization in the crystalline core (Cañaveras et al., 2006; Baskar et al., 2011), followed by relatively slow precipitation of clay-rich or organic-rich laminae in the shell (Borsato et al., 2000; Lacelle et al., 2004); this model is consistent with the presence of filamentous micro-organisms in the core of Doushantuo moonmilk (Figs. 3C–D). Modern botryoidal and flat crusts are mainly controlled by evaporation and condense processes rather than drip water, and this may also apply to the Doushantuo counterparts.

Modern karst studies indicated that the soil-ecosystem, which provides organic matter and CO_2 in the epikarst zone, is a prerequisite for the formation of speleothems (Kaufmann, 2003; Blyth et al., 2008). Elevated CO_2 concentrations in the soil-ecosystem are necessary for seeping groundwater to dissolve carbonate minerals and pick up alkalinity on its way to caves, and is also required for CO_2 degassing to drive speleothem precipitation when it leaves fissures. Critically, CO_2 concentration in the infiltrating water must be greater than CO_2 partial pressure in the cave atmosphere in order for speleothems to precipitate (White, 2005), and a soil-microbial ecosystem is the most parsimonious source of this elevated CO_2 concentration for the Doushantuo paleo-speleothems. Similarly, organic matter from the soil-microbial system provides a source of organic matter to account for the alternating organic-rich and organic-poor laminae in the Doushantuo paleo-speleothems. Therefore, the paleo-speleothems described here, together with the filamentous microfossils trapped in them (Figs. 3C–D), offer strong evidence for a speedy recovery of the terrestrial ecosystem and particularly the soil-microbial system in the aftermath of the Marinoan snowball Earth glaciation.

CONCLUSIONS

We report the wide distribution of silicified miniature paleo-speleothems from karstic sheet-cracks in the cap dolostone of the basal Ediacaran Doushantuo Formation in South China, which was deposited at ca. 635 Ma immediately after the terminal Cryogenian Marinoan snowball Earth glaciation. These speleothems include stalactites, stalagmites, helictites, moonmilk, botryoids, and flat crusts. They are interpreted to have formed during the post-glacial isostatic rebound, which drove the karstification of the cap dolostone. The speleothems were precipitated and then fully or partially silicified sometime between 635 Ma and 632 Ma, and more likely around 635 Ma. Insofar as speleothem precipitation critically depends on elevated CO_2 concentrations in the soil-ecosystem, the wide occurrence of speleothems in the Doushantuo cap dolostone, together with filamentous microfossils trapped in these speleothems, provides robust evidence for a rapid post-glacial recovery of the terrestrial ecosystem and invites the investigation of paleo-speleothems in equivalent cap dolostone in other continents.

ACKNOWLEDGMENTS

This research was supported by Chinese National Natural Science Foundation (41802027, 41873058, 41921002), Guizhou Province Natural Science and Technology Foundation [JZ(2015)2009], and Guizhou Education University. S.X. was supported by U.S. National Science Foundation (EAR- 2021207). T.G. acknowledges financial support from China Scholarship Council. We thank Chuanming Zhou for helpful discussion.

FIGURE CAPTIONS

Figure 1. Polished slab and thin section of silicified speleothems in sheet-cracks of Doushantuo cap dolostone at Beidoushan section. (A) Scanned image of polished slab, showing flat crusts, singular stalactites, coalesced stalactites, a stalagnate (where a stalactite meets a stalagmite), and quartz cement between speleothems. (B) Transmitted light microscopic (TLM) image of petrographic thin section, showing transverse and longitudinal sections of stalactites. (C–D) Epifluorescence light microscopic (ELM) images of areas marked in (B), showing bright organic-rich and dull organic-poor laminae. The following symbols and abbreviations apply to this and all other figures: white dot line, cap; white solid line, isopachous dolomite; black solid line, flat crust; black solid arrow, singular stalactite; black hollow arrow, coalesced stalactite; black dot line, stalagnate; red solid arrow, "soda straw" drip channel; white solid arrow, calcite laminae in incompletely silicified speleothem; cap, cap dolostone; ID, isopachous dolomite; QC, quartz cement; CR, flat crust.

Figure 2. Polished slab and thin sections of silicified stalagmites, stalactites, and flat crusts in sheet-cracks of Doushantuo cap dolostone at Wenghui section. (A) Digital image of polished slab, showing stalagmites, stalactites, and flat crusts. Stratigraphic up direction on top (blue arrow). (B) RLM image of petrographic thin section prepared from area marked in (A), showing stalagmites (longitudinal section) with mamillary aggregates (blue hollow arrows) and flat crusts. (D) TLM image of petrographic thin section prepared from area marked in (A), showing stalagmites, stalactites, and QC between paleo-speleothems. (C, E, F) ELM images of marked areas in (B) and (D), showing alternating bright organic-rich and dull organic-poor laminae, as well as "soda straw" drip channel in (F).

Figure 3. Petrographic thin sections of silicified helictites, moonmilks, flat crusts, and a partially silicified stalactite in sheet-cracks of Doushantuo cap dolostone at Beidoushan (A–D) and Xiaofenghe (E) sections. (A) ELM image showing flat crusts with vermiform-like helictites. (B) Backscattered scanning electron microscopic (BSEM) image of area marked in (A) showing central canals (red hollow arrows). (C) TLM image showing isopachous dolomite (ID) and moonmilk. (D) Enlargement of area marked in (C), showing filamentous microfossils (green arrows in C and D). (E) RLM image of partially silicified stalactite with residual calcite laminae (white solid arrows).

Figure 4. Polished slab, hand sample, and thin sections of silicified and partially silicified flat crusts and botryoids in sheet-cracks of Doushantuo cap dolostone at Beidoushan (A, E), Xiaofenghe (B), Wenghui (C), Zhangcunping (D), and Daping (F–H) sections. (A) Scanned image of polished slab showing flat crusts on sheet-crack walls, with a cap dolostone breccia in center. (B) TLM image showing cap dolostone, ID, and flat crusts. (C) TLM image showing flat crust laminae. (D) Hand sample showing botryoids (red double-headed arrow) and the mold of the botryoids (black double-headed arrow) in a sheet-crack filled by cements growing from upper right and lower right. A red dot line highlights the boundary between sheet-crack walls and botryoids. (E) TLM image showing botryoidal laminae overlying ID. (F) BSEM image showing partially silicified botryoids with calcitic laminae (white solid arrows) and siliceous replacement (white hollow arrows). (G) TLM image showing partially silicified organic-rich calcareous botryoidal laminae (white solid arrows) and silicified laminae (white hollow arrows). (H) ELM image of area marked in (G), showing bright organic-rich and dull organic-poor laminae.

Figure DR 1. Geological and paleogeographic maps showing sample localities, and stratigraphic columns of Ediacaran successions at Zhangcunping (ZCP), Xiaofenghe (XFH), Beidoushan (BDS), Daping (DP), and Wenghui (WH) sections, South China. (A) Map showing major tectonic units and sample localities. (B) Paleogeographic reconstruction showing depositional environments of sample localities. (C) Stratigraphic columns of sample localities. ZCP section modified from Zhou et al. (2017a); XFH section modified from Xiao et al. (2012).; BDS section modified from Nie et al. (2006); Xiao et al. (2014); WH section modified from Wang et al. (2016). Data sources of radiometric ages: 599.3 ± 4.2 Ma—Barfod et al. (2002), 609 ± 5 Ma—Zhou et al. (2017a), and 614.0 ± 7.6 Ma—Liu et al. (2009).

Figure DR 2. A model of sheet-crack, isopachous dolomite, and speleothem formation. (A) Post-glacial isostatic rebound made the cap dolostone to be exposed above sea-level. Dissolution, sheet-crack formation, and isopachous dolomite precipitation occurred in the phreatic zone. Speleothems were formed in sheet-cracks when the cap dolostone was elevated to the vadose zone. (B) A close-up of a sheet-crack in (A), showing six types of speleothems.

342 Fig. 1

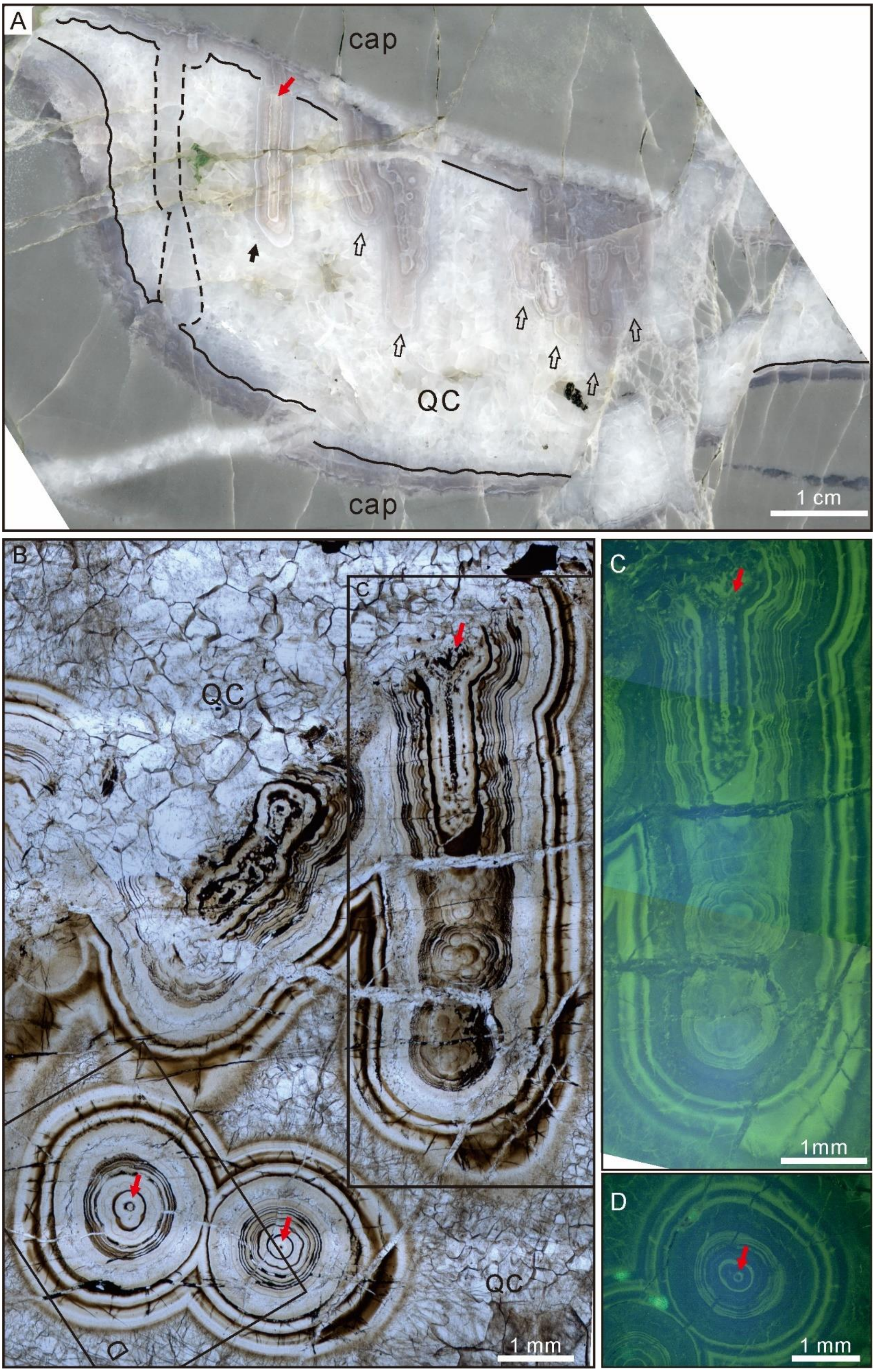

343

344 Fig. 2

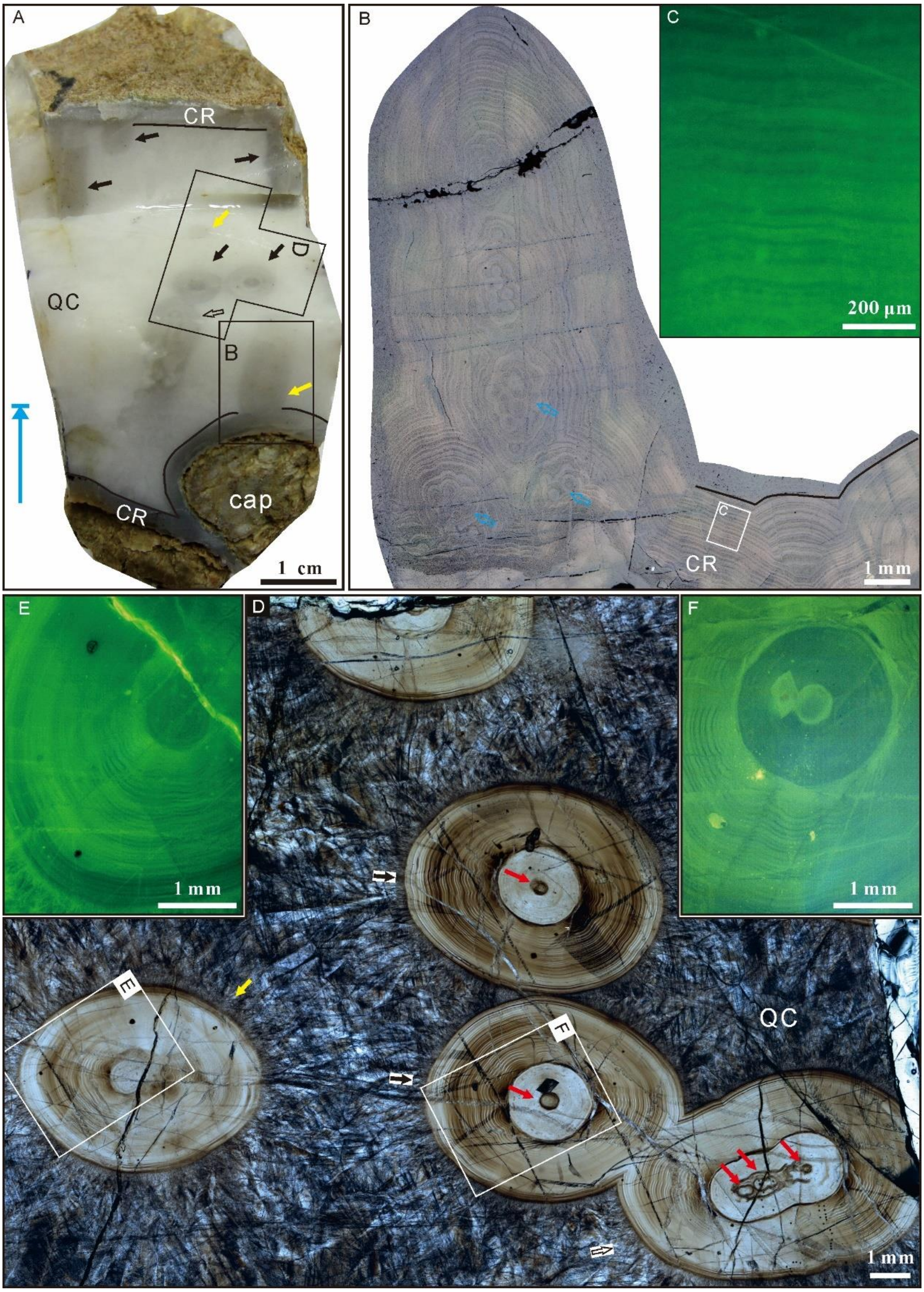

345

346

Fig. 3

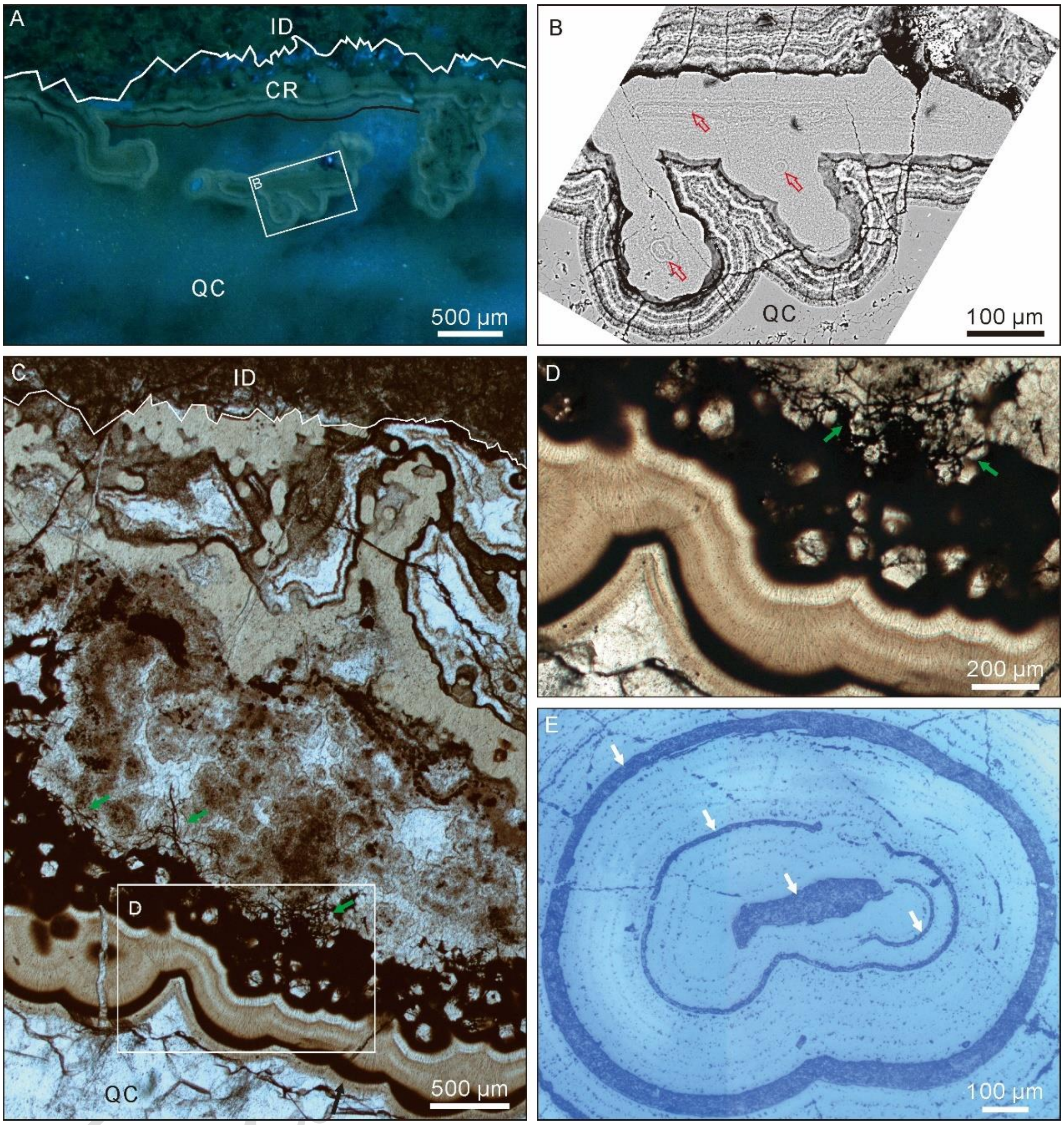

350 Fig. 4

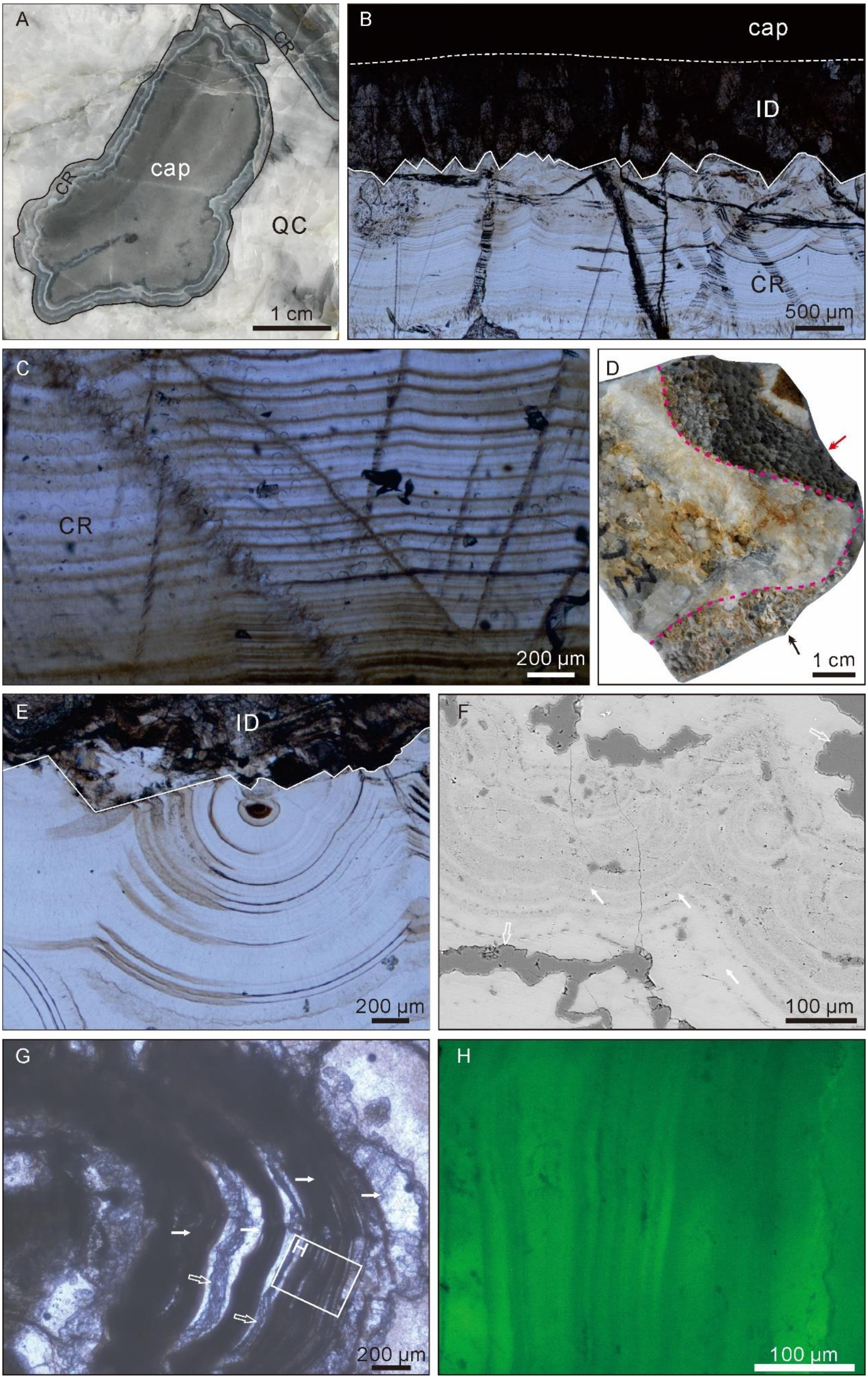
A
cap
CR
CR
QC
1 cm
B
cap
ID
CR
500 µm
C
CR
200 µm
D
1 cm
E
ID
200 µm
F
100 µm
G
H
200 µm
H
100 µm

351

Data Repository Figure 1

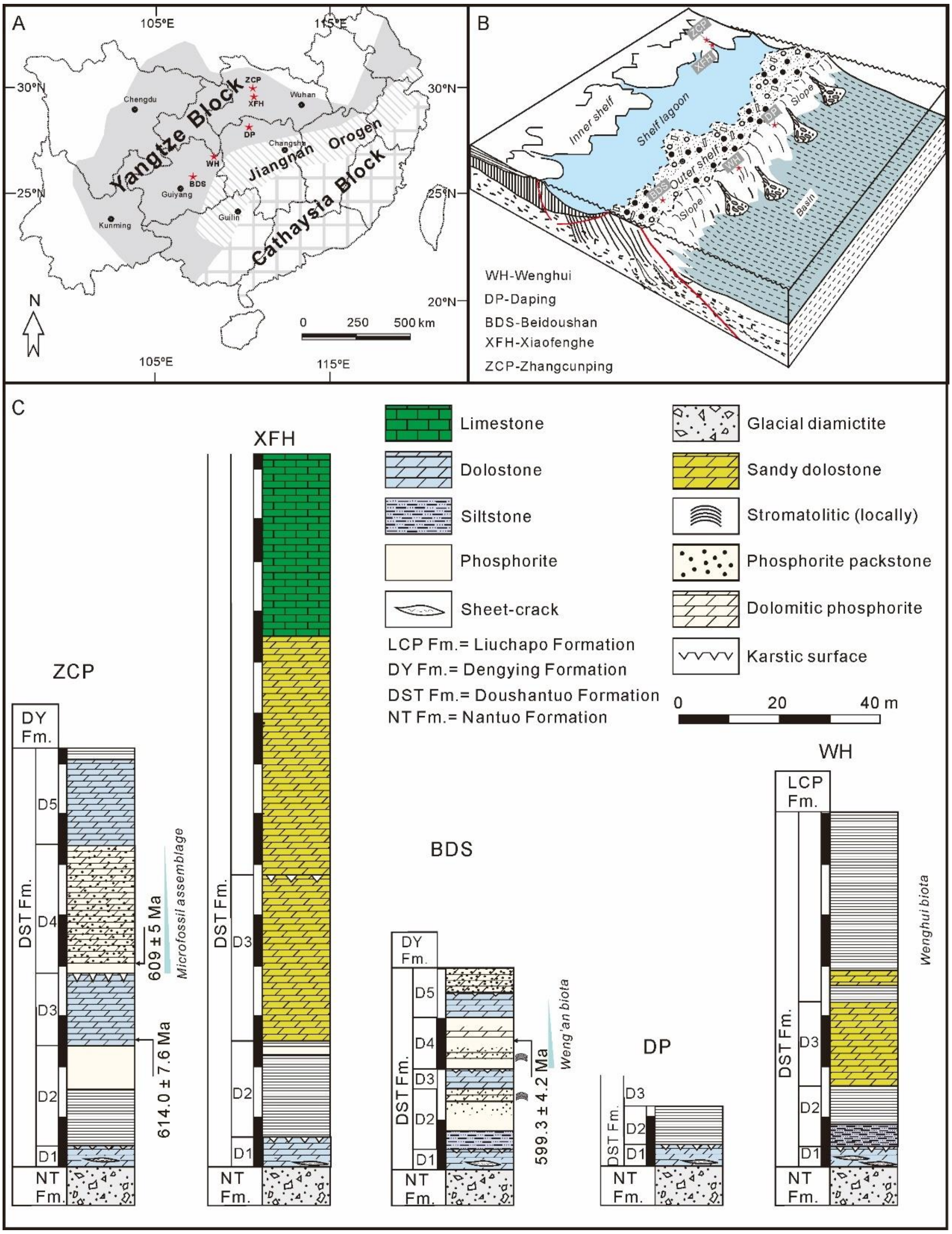

Data Repository Figure 2

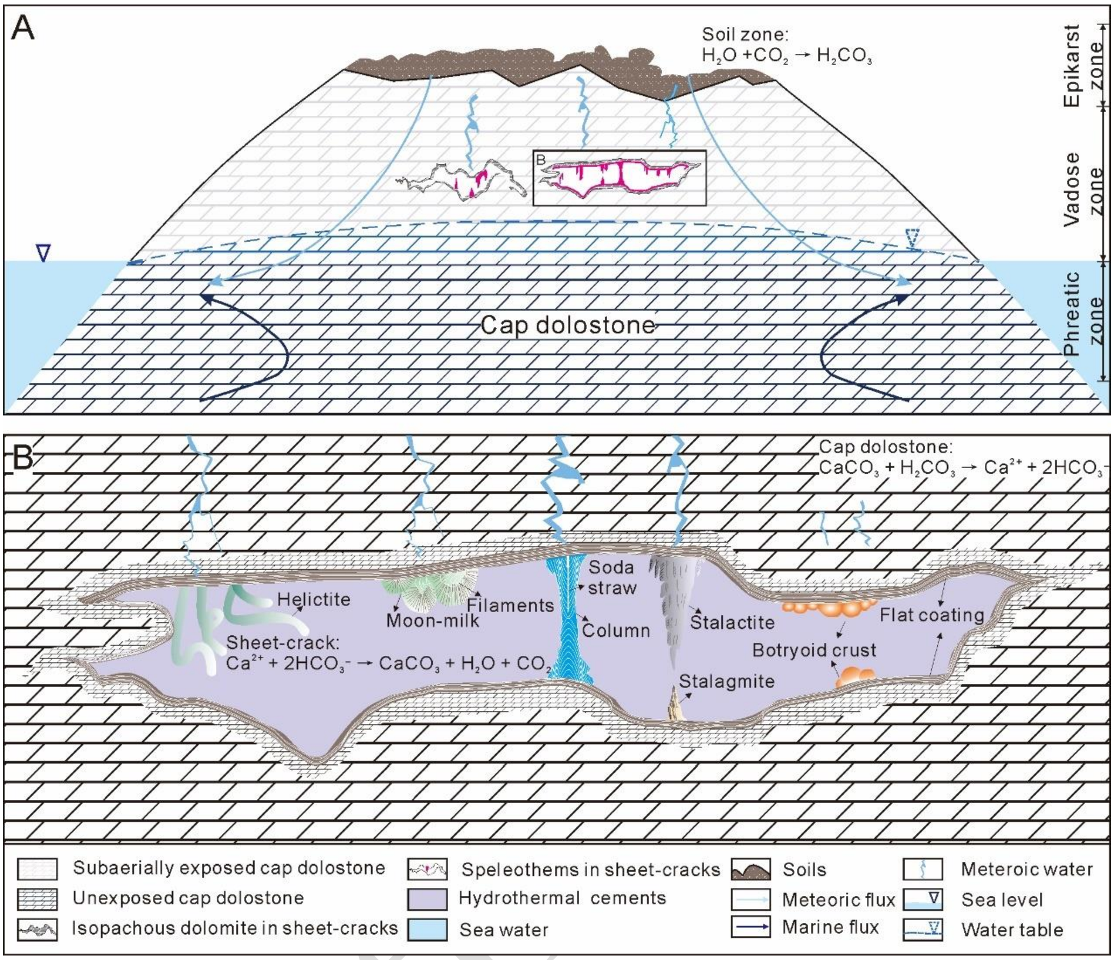

REFERENCES CITED

Álvaro, J. J., and Clausen, S., 2010, Morphology and ultrastructure of epilithic versus cryptic, microbial growth in lower Cambrian phosphorites from the Montagne Noire, France: Geobiology, v. 8, p. 89–100, doi:10.1111/j.1472-4669.2009.00229.x.

Amodio, S., Barattolo, F., and Riding, R., 2018, Early Cretaceous dendritic shrub-like fabric in karstified peritidal carbonates from southern Italy: Sedimentary Geology, v. 373, p. 134–146, doi:10.1016/j.sedgeo.2018.06.001.

Aubrecht, R., Brewer-Carías, C., Šmída, B., Audy, M., and Kováčik, Ľ., 2008, Anatomy of biologically mediated opal speleothems in the World's largest sandstone cave: Cueva Charles Brewer, Chimantá Plateau, Venezuela: Sedimentary Geology, v. 203, p. 181–195, doi:10.1016/j.sedgeo.2007.10.005.

Baker, A., Barnes, W. L., and Smart, P. L., 1996, Speleothern luminescence intensity and spectral characteristics: Signal calibration and a record of palaeovegetation change: Chemical Geology, v. 130, p. 65–76, doi:10.1016/0009-2541(96)00003-4.

Baker, A., Proctor, C. J., and Barnes, W. L., 2002, Stalagmite lamina doublets: a 1000 year proxy record of severe winters in northwest Scotland?: International Journal of Climatology, v. 22, p. 1339–1345, doi:10.1002/joc.800.

Baker, A., Smart, P. L., Edwards, R. L., and Richards, D. A., 1993, Annual growth banding in a cave stalagmite: Nature, v. 364, p. 518–520, doi:10.1038/364518a0.

Banks, V., and Jones, P., 2012, Hydrogeological significance of secondary terrestrial carbonate deposition in karst environments, *in* Gholam, A. K., ed., Hydrogeology-A Global Perspective: Janeza Trdine 9, 51000 Rijeka, Croatia, InTech, p. 43–78.

Barfod, G. H., Albarède, F., Knoll, A. H., Xiao, S., Télouk, P., Frei, R., and Baker, J., 2002, New Lu–Hf and Pb–Pb age constraints on the earliest animal fossils: Earth and Planetary Science Letters, v. 201, p. 203–212, doi:10.1016/s0012-821x(02)00687-8.

Baskar, S., Baskar, R., and Routh, J., 2011, Biogenic evidences of moonmilk deposition in the Mawmluh cave, Meghalaya, India: Geomicrobiology Journal, v. 28, p. 252–265, doi:10.1080/01490451.2010.494096.

Blyth, A. J., Baker, A., Collins, M. J., Penkman, K. E., Gilmour, M. A., Moss, J. S., Genty, D., and Drysdale, R. N., 2008, Molecular organic matter in speleothems and its potential as an environmental proxy: Quaternary Science Reviews, v. 27, p. 905–921, doi:10.1016/j.quascirev.2008.02.002.

Borsato, A., Frisia, S., Jones, B., and Van Der Borg, K., 2000, Calcite moonmilk: crystal morphology and environment of formation in caves in the Italian Alps: Journal of Sedimentary Research, v. 70, p. 1171–1182, doi:10.1306/032300701171.

Borsato, A., Frisia, S., Miorandi, R., van der Borg, K., Spötl, C., and Corradini, F., 2007, Holocene climate and environmental reconstruction from calcareous tufa and moonmilk deposits in Trentino caves: Acta Geologica, v. 83, p. 239–260.

Brook, G. A., Rafter, M. A., Railsback, L. B., Sheen, S.-W., and Lundberg, J., 1999, A high-resolution proxy record of rainfall and ENSO since AD 1550 from layering in stalagmites from Anjohibe Cave, Madagascar: The Holocene, v. 9, p. 695–705, doi:10.1191/095968399677907790.

Cañaveras, J. C., Cuezva, S., Sanchez-Moral, S., Lario, J., Laiz, L., Gonzalez, J. M., and Saiz-Jimenez, C., 2006, On the origin of fiber calcite crystals in moonmilk deposits: Naturwissenschaften, v. 93, p. 27–32, doi:10.1007/s00114-005-0052-3.

Cao, R., Tang, T., Xue, Y., Yu, C., Yin, L., and Zhao, W., 1989, Research on Sinian Strata with ore deposits in the Yangzi (Yangtze) region, China: Upper Precambrian of the Yangzi (Yangtze) Region, China. Nanjing University Press, Nanjing, p. 1–94.

Condon, D., Zhu, M., Bowring, S., Wang, W., Yang, A., and Jin, Y., 2005, U-Pb Ages from the Neoproterozoic Doushantuo Formation, China: Science, v. 308, p. 95–98, doi:10.1126/science.1107765.

Cruz, F. W., Burns, S. J., Karmann, I., Sharp, W. D., Vuille, M., and Ferrari, J. A., 2006, A stalagmite record of changes in atmospheric circulation and soil processes in the Brazilian subtropics during the Late Pleistocene: Quaternary Science Reviews, v. 25, p. 2749–2761, doi:10.1016/j.quascirev.2006.02.019.

Cui, Y., Lang, X., Li, F., Huang, K., Ma, H., Li, C., Pei, H., Li, C., Zhou, C., and Shen, B., 2019, Germanium/silica ratio and rare earth element composition of silica-filling in sheet cracks of the Doushantuo cap carbonates, South China: Constraining hydrothermal activity during the Marinoan snowball Earth glaciation: Precambrian Research, v. 332, p. 105407, doi:10.1016/j.precamres.2019.105407.

Dörr, H., and Münnich, K. O., 1986, Annual Variations of the ^{14}C Content of Soil CO_2: Radiocarbon, v. 28, p. 338–345, doi:10.1017/S0033822200007438.

Dreybrodt, W., and Romanov, D., 2008, Regular stalagmites: The theory behind their shape: Acta Carsologica, v. 37, p. 175–184, doi:10.3986/ac.v37i2-3.145.

Fairchild, I. J., and Baker, A., 2012, Speleothem science: From process to past environments, *in* Bradley, R., ed., The architecture of speleothems, Volume 3:

The Atrium, Southern Gate, Chichester, West Sussex, PO19 8SQ, UK, John Wiley & Sons, p. 213–222.

Fairchild, I. J., Smith, C. L., Baker, A., Fuller, L., Spötl, C., Mattey, D., McDermott, F., and E.I.M.F, 2006, Modification and preservation of environmental signals in speleothems: Earth-Science Reviews, v. 75, p. 105–153, doi:10.1016/j.earscirev.2005.08.003.

Freytet, P., and Verrecchia, E. P., 2002, Lacustrine and palustrine carbonate petrography: an overview: Journal of Paleolimnology, v. 27, p. 221–237, doi:10.1023/A:1014263722766.

Frisia, S., and Borsato, A., 2010, Chapter 6 Karst, *in* Alonso-Zarza, A. M., and Tanner, L. H., eds., Developments in Sedimentology, Volume 61, Elsevier, p. 269–318.

Gams, I., and Beck Barry, F. E., 1981, Contribution to morphometrics of stalagmites, Proceedings of the 8th International Congress of Speleology, Volume 8, p. 276–278.

Gribovszki, K., Kovács, K., Mónus, P., Bokelmann, G., Konecny, P., Lednická, M., Moseley, G., Spötl, C., Edwards, R. L., Bednárik, M., Brimich, L., and Tóth, L., 2017, Estimating the upper limit of prehistoric peak ground acceleration using an in situ, intact and vulnerable stalagmite from Plavecká priepast cave (Detrekői-zsomboly), Little Carpathians, Slovakia—first results: Journal of Seismology, v. 21, p. 1111–1130, doi:10.1007/s10950-017-9655-3.

Hoffman, P. F., Abbot, D. S., Ashkenazy, Y., Benn, D. I., Brocks, J. J., Cohen, P. A., Cox, G. M., Creveling, J. R., Donnadieu, Y., Erwin, D. H., Fairchild, I. J., Ferreira, D., Goodman, J. C., Halverson, G. P., Jansen, M. F., Le Hir, G., Love, G. D., Macdonald, F. A., Maloof, A. C., Partin, C. A., Ramstein, G., Rose, B. E. J., Rose, C. V., Sadler, P. M., Tziperman, E., Voigt, A., and Warren, S. G., 2017, Snowball Earth climate dynamics and Cryogenian geology-geobiology: Science Advances, v. 3, p. e1600983, doi:10.1126/sciadv.1600983.

Horodyski, R. J., and Knauth, L. P., 1994, Life on land in the Precambrian: Science, v. 263, p. 494–498, doi:10.1126/science.263.5146.494.

Huff, L. C., 1940, Artificial helictites and gypsum flowers: The Journal of Geology, v. 48, p. 641–659, doi:10.1086/624919.

James, N. P., Narbonne, G. M., and Kyser, T. K., 2001, Late Neoproterozoic cap carbonates: Mackenzie Mountains, northwestern Canada: precipitation and global glacial meltdown: Canadian Journal of Earth Sciences, v. 38, p. 1229–1262, doi:10.1139/e01-046.

Jiang, G., Kennedy, M. J., Christie-Blick, N., Wu, H., and Zhang, S., 2006, Stratigraphy, sedimentary structures, and textures of the late Neoproterozoic Doushantuo cap carbonate in South China: Journal of Sedimentary Research, v. 76, p. 978–995, doi:10.2110/jsr.2006.086.

Kaufmann, G., 2003, Stalagmite growth and palaeo-climate: the numerical perspective: Earth and Planetary Science Letters, v. 214, p. 251–266, doi:10.1016/S0012-821X(03)00369-8.

Kennedy, M., Droser, M., Mayer, L. M., Pevear, D., and Mrofka, D., 2006, Late Precambrian oxygenation; inception of the clay mineral factory: Science, v. 311, p. 1446–1449, doi:10.1126/science.1118929.

Knauth, L. P., and Kennedy, M. J., 2009, The late Precambrian greening of the Earth: Nature, v. 460, p. 728–732, doi:10.1038/nature08213.

Kump, L. R., 2014, Hypothesized link between Neoproterozoic greening of the land surface and the establishment of an oxygen-rich atmosphere: Proceedings of the National Academy of Sciences, v. 111, p. 14062–14065,

doi:10.1073/pnas.1321496111.
Lacelle, D., Lauriol, B., and Clark, I. D., 2004, Seasonal isotopic imprint in moonmilk from Caverne de l'Ours (Quebec, Canada): implications for climatic reconstruction: Canadian Journal of Earth Sciences, v. 41, p. 1411–1423, doi:10.1139/e04-080.
Lin, Y., Zhang, M., Qin, J., Zhu, X., and Cheng, H., 2005, Growth rate of cave stalagmite: Geological Review, v. 51, p. 435–442.
Liu, P., Yin, C., Gao, L., Tang, F., and Chen, S., 2009, New material of microfossils from the Ediacaran Doushantuo Formation in the Zhangcunping area, Yichang, Hubei Province and its zircon SHRIMP U-Pb age: Chinese Science Bulletin, v. 54, p. 1058–1064, doi:10.1007/s11434-008-0589-6.
McDermott, F., 2004, Palaeo-climate reconstruction from stable isotope variations in speleothems: a review: Quaternary Science Reviews, v. 23, p. 901–918, doi:10.1016/j.quascirev.2003.06.021.
Nie, W., Ma, D., Pan, J., Zhou, J., and Wu, K., 2006, $\delta^{13}C$ excursions of phosphorite-bearing rocks in Neoproterozoic-Early Cambrian interval in Guizhou, South China: implications for palaeoceanic evolutions: Journal of Nanjing University (Natural Sciences), v. 42, p. 257–268.
Onuk, P., Dietzel, M., and Hauzenberger, C. A., 2014, Formation of helictite in the cave Dragon Belly (Sardinia, Italy)—Microstructure and incorporation of Mg, Sr, and Ba: Geochemistry, v. 74, p. 443–452, doi:10.1016/j.chemer.2014.04.003.
Qing, H., and Nimegeers, A. R., 2008, Lithofacies and depositional history of Midale carbonate-evaporite cycles in a Mississippian ramp setting, Steelman-Bienfait area, southeastern Saskatchewan, Canada: Bulletin of Canadian Petroleum Geology, v. 56, p. 209–234, doi:10.2113/gscpgbull.56.3.209.

Railsback, L. B., Liang, F., Brook, G. A., Voarintsoa, N. R. G., Sletten, H. R., Marais, E., Hardt, B., Cheng, H., and Edwards, R. L., 2018, The timing, two-pulsed nature, and variable climatic expression of the 4.2 ka event: A review and new high-resolution stalagmite data from Namibia: Quaternary Science Reviews, v. 186, p. 78–90, doi:10.1016/j.quascirev.2018.02.015.

Romero, G. R., Sanchez, E. A. M., Soares, J. L., Nogueira, A. C. R., and Fairchild, T. R., 2020, Waxing and waning of microbial laminites in the aftermath of the Marinoan glaciation at the margin of the Amazon Craton (Brazil): Precambrian Research, v. 348, p. 105856, doi:10.1016/j.precamres.2020.105856.

Shields, G. A., Deynoux, M., Strauss, H., Paquet, H., and Nahon, D., 2007, Barite-bearing cap dolostones of the Taoudéni Basin, northwest Africa: Sedimentary and isotopic evidence for methane seepage after a Neoproterozoic glaciation: Precambrian Research, v. 153, p. 209–235, doi:10.1016/j.precamres.2006.11.011.

Skotnicki, S. J., and Knauth, L. P., 2007, The Middle Proterozoic Mescal Paleokarst, Central Arizona, U.S.A.: Karst Development, Silicification, and Cave Deposits: Journal of Sedimentary Research, v. 77, p. 1046–1062, doi:10.2110/jsr.2007.094.

Strother, P. K., Battison, L., Brasier, M. D., and Wellman, C. H., 2011, Earth's earliest non-marine eukaryotes: Nature, v. 473, p. 505–509, doi:10.1038/nature09943.

Tan, L., Yi, L., Cai, Y., Shen, C.-C., Cheng, H., and An, Z., 2013, Quantitative temperature reconstruction based on growth rate of annually-layered stalagmite: a case study from central China: Quaternary Science Reviews, v. 72, p. 137–145, doi:10.1016/j.quascirev.2013.04.022.

Tan, M., Baker, A., Genty, D., Smith, C., Esper, J., and Cai, B., 2006, Applications of stalagmite laminae to paleoclimate reconstructions: Comparison with dendrochronology/climatology: Quaternary Science Reviews, v. 25, p. 2103–2117, doi:10.1016/j.quascirev.2006.01.034.

Thomazo, C., Couradeau, E., and Garcia-Pichel, F., 2018, Possible nitrogen fertilization of the early Earth Ocean by microbial continental ecosystems: Nat Commun, v. 9, p. 2530, doi:10.1038/s41467-018-04995-y.

van der Heijden, M. G. A., Bardgett, R. D., and van Straalen, N. M., 2008, The unseen majority: soil microbes as drivers of plant diversity and productivity in terrestrial ecosystems: Ecology Letters, v. 11, p. 296–310, doi:10.1111/j.1461-0248.2007.01139.x.

van Maldegem, L. M., Sansjofre, P., Weijers, J. W. H., Wolkenstein, K., Strother, P. K., Wörmer, L., Hefter, J., Nettersheim, B. J., Hoshino, Y., Schouten, S., Sinninghe Damsté, J. S., Nath, N., Griesinger, C., Kuznetsov, N. B., Elie, M., Elvert, M., Tegelaar, E., Gleixner, G., and Hallmann, C., 2019, Bisnorgammacerane traces predatory pressure and the persistent rise of algal ecosystems after Snowball Earth: Nat Commun, v. 10, p. 476, doi:10.1038/s41467-019-08306-x.

Verheyden, S., Keppens, E., Fairchild, I. J., McDermott, F., and Weis, D., 2000, Mg, Sr and Sr isotope geochemistry of a Belgian Holocene speleothem: implications for paleoclimate reconstructions: Chemical Geology, v. 169, p. 131–144, doi:10.1016/S0009-2541(00)00299-0.

Wang, Y., Wang, Y., Du, W., and Wang, X., 2016, New Data of Macrofossils in the Ediacaran Wenghui Biota from Guizhou, South China: Acta Geologica Sinica - English Edition, v. 90, p. 1611–1628, doi:10.1111/1755-6724.12805.

Wellman, C. H., and Strother, P. K., 2015, The terrestrial biota prior to the origin of land plants (embryophytes): a review of the evidence: Palaeontology, v. 58, p. 601–627, doi:10.1111/pala.12172.

White, W. B., 2005, Speleothems, *in* White, W. B., Culver, D. C., and Pipan, T., eds., Encyclopedia of caves: SPi Global, India, Academic Press, p. 1006–1017.

Xiao, S., McFadden, K. A., Peek, S., Kaufman, A. J., Zhou, C., Jiang, G., and Hu, J., 2012, Integrated chemostratigraphy of the Doushantuo Formation at the northern Xiaofenghe section (Yangtze Gorges, South China) and its implication for Ediacaran stratigraphic correlation and ocean redox models: Precambrian Research, v. 192-195, p. 125–141, doi:10.1016/j.precamres.2011.10.021.

Xiao, S., Muscente, A., Chen, L., Zhou, C., Schiffbauer, J. D., Wood, A. D., Polys, N. F., and Yuan, X., 2014, The Weng'an biota and the Ediacaran radiation of multicellular eukaryotes: National Science Review, v. 1, p. 498–520, doi:10.1093/nsr/nwu061.

Zhao, Y., Zhao, M., and Li, S., 2018, Evidences of hydrothermal fluids recorded in microfacies of the Ediacaran cap dolostone: Geochemical implications in South China: Precambrian Research, v. 306, p. 1–21, doi:10.1016/j.precamres.2017.12.028.

Zhou, C., Bao, H., Peng, Y., and Yuan, X., 2010, Timing the deposition of ^{17}O-depleted barite at the aftermath of Nantuo glacial meltdown in South China: Geology, v. 38, p. 903–906, doi:10.1130/G31224.1.

Zhou, C., Lang, X., Huyskens, M. H., Yin, Q.-Z., and Xiao, S., 2019, Calibrating the terminations of Cryogenian global glaciations: Geology, v. 47, p. 251–254, doi:10.1130/g45719.1.

Zhou, C., Li, X., Xiao, S., Lan, Z., Ouyang, Q., Guan, C., and Chen, Z., 2017a, A new SIMS zircon U–Pb date from the Ediacaran Doushantuo Formation: age constraint on the Weng'an biota: Geological Magazine, v. 154, p. 1193–1201, doi:10.1017/S0016756816001175.

Zhou, G., Luo, T., Zhou, M., Xing, L., and Gan, T., 2017b, A ubiquitous hydrothermal episode recorded in the sheet-crack cements of a Marinoan cap dolostone of South China: Implication for the origin of the extremely ^{13}C-depleted calcite cement: Journal of Asian Earth Sciences, v. 134, p. 63–71, doi:10.1016/j.jseaes.2016.11.007.